THE JOURNAL OF PHYSICAL CHEMISTRY A
Article
Cite This: J. Phys. Chem. A 2019, 123, 9199−9208
pubs.acs.org/JPCA

Experimental and Theoretical Study of Surface-Enhanced Raman Spectra of Sulfadiazine Adsorbed on Nanoscale Gold Colloids

Xiao-Ru Shen,[†] Hong Zheng,[‡] Ran Pang,[†] Guo-Kun Liu,*[,‡] De-Yin Wu,*[,†] and Zhong-Qun Tian[†]

[†]State Key Laboratory of Physical Chemistry of Solid Surface, Collaborative Innovation Center of Chemistry for Energy Materials, and Department of Chemistry, College of Chemistry and Chemical Engineering, Xiamen University, Xiamen 361005, China

[‡]Department of the Environment & Ecology, State Key Laboratory of Marine Environmental Science, Xiamen University, Xiamen 361102, China

Supporting Information

ABSTRACT: Sulfadiazine, as a class of antibiotics, has been widely used in the world for decades; however, its surface-enhanced Raman spectra (SERS) on gold colloids are obviously different from ordinary Raman spectra in the solid powder and liquid solution. To explore the reasons for such significant differences, we used density functional theory calculations and normal-mode analysis to investigate the effects of the configuration, conformation, protonation, hydrogen-bonding interaction, and adsorption configurations of sulfadiazine on gold clusters to check these different effects on the vibrational assignments. Our calculated results can be summarized as two points. First, the Raman spectra strongly depend on the configuration, conformation, protonation, and hydrogen bonding of sulfadiazine. Second, the wagging vibration displays a significant vibrational frequency shift and a very strong SERS peak responsible for the observed SERS signal when sulfadiazine is adsorbed on gold clusters through the terminal amino group. This is different from another adsorption configuration through two oxygen atoms of the $-SO_2NH-$ group on gold clusters. Finally, we further investigate the potential energy surfaces along the wagging vibration and the binding interaction of $-NH_2$ adsorbed on different sites of gold surfaces.

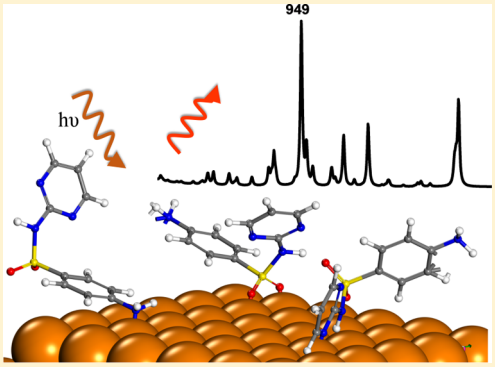

1. INTRODUCTION

Sulfadiazine plays an important role in treating infectious diseases, protecting human health and promoting the development of food industry.[1−4] The medicines have considerable medical significance, and their preparation accounts for a large part of the pharmaceutical industry,[5] but the overuse of antibiotics has shown negative effects. Its potential risks involve drug resistance and damage to human organs, leading to double infection and causing social harm.[6] Therefore, it is urgent to improve the accuracy of sulfadiazine detection. At present, the detection techniques of sulfadiazine are mainly divided into two categories: one is in vivo detection in poultry and other organisms, mainly biosensors, by fluorescence immunoassays.[7] The other is in vitro analysis of soil, sewage, and other materials. The main methods include an intermittent equilibrium method, which detects according to the adsorption and desorption behavior of detectors.[8] However, these detection techniques need long-time pretreatment procedures and complex detection; more simple and convenient detection methods for sulfadiazine are urgently needed.

Raman spectroscopy based on the Raman scattering effect is a powerful method to identify molecular fingerprint information for qualitative and quantitative analyses and structural characterization of molecules. In particular, surface-enhanced Raman spectroscopy (SERS) has a huge enhancement effect on the Raman scattering cross section of probe molecules adsorbed on rough noble electrodes.[9] The SERS enhancement effect is an optical physical phenomenon with higher detection sensitivity closely related to the properties of nanostructures, like the size, shape, and aggregation states of metal materials. Usually, the nanostructures of noble metals such as Ag, Au, and Cu can produce 10^5-10^{10} times more enhancement compared to the normal Raman spectral signal of the same probing molecule in solutions. Accordingly, the SERS has been considered as a highly sensitive probe to detect and identify sulfadiazine adsorbed on silver and gold surfaces.[10] However, its SERS spectra strongly dependent on experimental conditions are different from normal Raman spectra in complex environments.[11,12] It is necessary comprehensively to build the accurate relationship of the Raman spectrum, SERS, and microscopic structure information of free sulfadiazine and adsorbed sulfadiazine on silver and gold surfaces.

From the first-principles quantum mechanics, ab initio approach, and density functional theoretical (DFT) calculations,[13,14] one can determine molecular geometric structures, vibrational spectra, and thermodynamic properties at molecular levels.[15,16] As one of the most important sulfonamides,

Received: August 1, 2019
Revised: September 13, 2019
Published: September 24, 2019

DOI: 10.1021/acs.jpca.9b07346
J. Phys. Chem. A 2019, 123, 9199−9208

sulfadiazine has been studied for a long time.[17] Some experimental and theoretical studies of sulfadiazine and sulfanilamide have been reported,[12,18−21] but a complete analysis of SERS data is still quite lacking. In our previous studies, we investigated the normal Raman spectra and SERS of aniline,[22] benzyl,[23] and *p*-aminothiophenol[11] and provided significant insight into the relation of Raman and SERS spectra as well as microscopic structures in a liquid solution and on metal surfaces. Now, we extend our study to a more complex modeling molecule, sulfadiazine, which involves not only configuration and conformational isomerization, protonation, and hydrogen-bonding interaction but also adsorption orientation to influence Raman spectral properties.

In this work, we first present normal Raman spectra in solid powder and aqueous solution and SERS of sulfadiazine adsorbed on gold colloids. There is a significant difference between normal Raman and SERS spectra. Then, we carried out systematically theoretical calculations and vibrational analysis to examine the conformation of sulfadiazine and identify the corresponding relation between its structural characteristics and Raman spectrum information. Finally, we further explore the adsorption structures of sulfadiazine on different gold clusters based on the molecule-metal cluster model. The present theoretical and experimental results reveal the nature of Raman spectra related to microscopic structures and interface chemical interactions in complex environments.

2. EXPERIMENTAL AND THEORETICAL METHODS

2.1. Reagents and Materials. Hydrochloric acid, nitric acid, chloroauric acid, and sodium chloride were purchased from Sinopharm Chemical Reagent Co. Ltd. Sulfadiazine was purchased from Shanghai McLean Biochemical Technology Co., Ltd. The sulfadiazine standard reserve solution (1 g/L) was disposed in hydrochloric acid solution (1:1 v/v) and stored in dark at low temperature, and the sulfadiazine standard solution of other concentrations was diluted by Millipore water. The glass instruments used in the experiment were soaked in aqua regia for 30 min and then cleaned with ultrapure water.

2.2. Raman Measurement Instruments and SERS Measurements. A WTEK Raman spectrometer (B&W Tek, China), including an i-Raman Plus Raman spectrometer, a BA C102-785 Raman laser probe, and a BAC151B microscope, was used.

AuNPs were synthesized using a simple method as described previously;[24,25] 1.5 mL of presynthesized AuNPs (Section S1, Supporting Information) was centrifuged in a centrifugal tube at a speed of 4000 rpm for 5 min. After removing the supernatant, concentrated AuNPs were obtained for later use.

Then, sulfadiazine (1 mg/L), NaCl (1 mol/L), and the concentrated AuNPs sol were added to a 96-well plate in a certain proportion and mixed thoroughly (the total volume of the mixed solution was 250−300 μL). SERS signals were excited by a 785 nm laser. The acquisition time was 2 s, and the accumulation time was 10 cycles. The SERS spectra were recorded for qualitative analysis of the tested samples.

2.3. Computational Details. From the sulfadiazine crystal structure,[26] we first build the initial structures around the $-SO_2NH-$ group; one end is the aniline ring and the other end is the pyrimidine ring. Thus, the molecule can produce two conformations around the N−S bond, as shown in Figure 2iso-a and iso-b. Meanwhile, hydrogen atoms as well as the nitrogen atoms of pyrimidine rings may be isomerized into two configurations on the imine through hydrogen-bonding interaction.[27]

Different functional methods were used to optimize the geometric structures, compared to the structural parameters determined from X-ray crystal structures[27] and gas-phase electron diffraction.[28] We used hybrid functionals B3LYP,[29−32] CAM-B3LYP,[33] B3P86,[34] and M06[35] and ab initio MP2[36−38] approach to calculate the stable conformations of sulfadiazine. The basis set used here was 6-311+G(d,p) for C, N, O, S, and H atoms of the investigated molecules.[39,40] For the Au atom, we adopted the small-core pseudopotential basis set, LANL2DZ, and the corresponding relativistic effective core potentials to describe the valence electrons and electrons in the inner shells, respectively.[41] Finally, the CAM-B3LYP, 6-311+G(d,p) approach was used to further calculate optimized structures and Raman spectra of sulfadiazine in aqueous solution and interacting with gold clusters.

Taking the solvation effect into account, the polarizable continuum model (PCM) was used in this work,[42] which includes a solvent reaction field self-consistent with the solute electrostatic potential. According to the possible factors influencing Raman spectra of sulfadiazine in aqueous solution, we considered three cases, monomers, dimers, and protonated isomers, in aqueous solutions. Because a sulfadiazine molecule contains oxygen and nitrogen atoms, it can form intermolecular hydrogen bonds in solids and aqueous solutions. To study the influence of the intermolecular interaction more clearly on Raman spectra, we selected the lowest-energy configuration of a monomer to form four possible dimer structures and calculate their simulated Raman spectra.

For possible adsorption of sulfadiazine on gold, we assumed that it first adsorbs through the $-SO_2NH-$ group and the amino group. The former was proposed in a previous study for sulfanilamide adsorbed on silver surfaces.[18] According to our previous studies on aniline,[22] benzyl,[23] and *p*-aminothiophenol,[11] we guessed the possible adsorption through the amino nitrogen on gold clusters. The amino nitrogen can form a chemisorption state on gold surfaces. The later adsorption configuration is very consistent with the observed SERS spectra. However, this is very sensitive to the adsorption binding with metallic clusters. Our finding is that the weak binding interaction is better to simulate the observed SERS of sulfadiazine on gold colloids. The further DFT calculations are based on the orbital interaction and the potential energy surface to support the above finding. Full geometry optimizations and frequency analyses were carried out using Gaussian09 package.[43]

The scaled quantum mechanic force field procedure was used to clarify the assignment of the fundamentals on the basis of the potential energy distribution (PED) using Scale 2.0 program.[44,45] To compare calculated vibrational frequencies with observed Raman peaks, we used the scaling factors of 0.981 for vibrational frequencies less than 2000 cm^{-1} and 0.967 for above 2000 cm^{-1}.[46] After the systematic corrections, the mean deviation between theoretical and experimental vibrational frequencies decreases from 23 to 3 cm^{-1}.

To compare simulated and observed Raman spectra, we estimated the Raman intensity using the differential Raman scattering cross section of each vibrational mode.[47] In this case, Raman intensity is given as

DOI: 10.1021/acs.jpca.9b07346
J. Phys. Chem. A 2019, 123, 9199−9208

$$I_{\text{Raman}} = \frac{(2\pi)^4}{45}\frac{h}{8\pi^2 c\omega_i}\frac{(\omega_0-\omega_i)^4}{1-\exp(-hc\omega_i/k_BT)}\left[45\left(\frac{d\alpha}{dQ_i}\right)^2 + 7\left(\frac{d\gamma}{dQ_i}\right)^2\right] = \frac{(2\pi)^4}{45}\frac{h}{8\pi^2 c\omega_i}\frac{(\omega_0-\omega_i)^4}{1-\exp(-hc\omega_i/k_BT)}S_i$$

where h, c, k_B, and T are the Planck constant, light speed, Boltzmann constant, and Kelvin temperature, respectively. Here, ω_0 and ω_i denote the frequency (in cm^{-1}) of the incident light and the vibrational frequency of the ith mode, respectively. S_i is the Raman scattering factor that can be calculated using Gaussian09 at the equilibrium geometry.

3. RESULTS AND DISCUSSION

3.1. Experimental Raman and SERS Spectra. Figure 1a presents SERS of sulfadiazine adsorbed on gold surfaces of nanoparticles. For convenient comparison, we also recorded ordinary Raman spectra of sulfadiazine in an aqueous solution (Figure 1b) and in a solid powder (Figure 1c). In the normal Raman spectrum of solid powder, there are five characteristic peaks at 845, 992, 1096, 1148, and 1595 cm^{-1}. By inspecting the Raman spectra in the aqueous solution, we can notice that there are two red shift peaks from 845 to 804 cm^{-1} and from 1148 to 1122 cm^{-1}. For the SERS spectrum (Figure 1a), however, there are two strong peaks at 949 and 1580 cm^{-1}, where the strongest characteristic peak appears at 949 cm^{-1}. This is very different from the normal Raman spectra and the observed SERS spectrum of sulfadiazine adsorbed on silver.[48] To understand the significant difference, we next investigated systemically the relation between Raman spectra and microscopic structures using DFT calculations and normal-mode analysis.

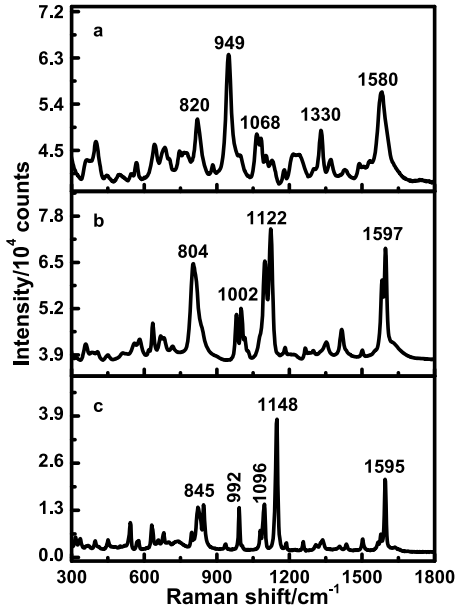

Figure 1. SERS and ordinary Raman spectra of sulfadiazine. (a) SERS on gold; (b) Raman spectrum recorded in an aqueous solution; and (c) Raman spectrum recorded in a solid powder.

3.2. Stable Isomers and Their Raman Spectra. Sulfadiazine can form four low-energy isomers. Figure 2i shows the experimental Raman spectrum of sulfadiazine in a solid powder and simulated Raman spectra of the four low-energy isomers of sulfadiazine (iso-a to iso-d). From DFT calculations, we first obtained two stable conformations rotating around the N−S bond, denoted iso-a and iso-b. We need to emphasize that the iso-a isomer was observed in the crystal structure.[26] Considering that the hydrogen of the −NH− isomerization in amide and pyrimidine moieties may form an intramolecular hydrogen bond, we can optimize two configuration isomers, denoted iso-c and iso-d. The relative energies of these four isomers increase from iso-a to iso-d (see Table S2). Compared with the experimental spectra of the solid powder (Figure 1c), our calculated Raman peak of the out-of-plane bending vibration of the amino group is stronger in the low-wavenumber region, whereas the other peaks are very well consistent with the experimental spectra. In particular, among the four isomers, the vibrational frequency and relative Raman intensity from the iso-a isomer are the most consistent with the experimental spectrum. Therefore, further DFT calculations will adopt the configuration iso-a in the latter text.

Simulated Raman spectra recorded using different hybrid functional methods and the ab initio MP2 method are shown in Figure 2ii. Table 1 lists their structural parameters compared with gas-phase electron diffraction[28] and crystal structures.[27] Among all theoretical structures, the structures obtained by the CAM-B3LYP method are in the best agreement with the experimental values of gas-phase electron diffraction[28] and crystal structures.[27] By inspecting the simulated Raman spectra shown in Figure 2ii, we can notice that the CAM-B3LYP functional method can also predict the characteristic Raman peaks of the most stable isomer. Therefore, we used the CAM-B3LYP functional method for the later calculations. It is worth noticing that the CAM-B3LYP functional predicts a higher Raman frequency at 1646 than at 1602 cm^{-1} compared to the B3LYP functional (see Figure S1). However, it is better to predict the characteristic frequency of the sulfonamide group.

3.3. Vibrational Analysis. Until now, there was a lack of a complete vibrational assignment of sulfadiazine in the literature. We have provided a complete vibrational assignment based on the scaled quantum force field method combining the optimized structures and corresponding force constants. Our calculated results of sulfadiazine and its atomic label are completely summarized in the Supporting Information (see Table S1) and Table 1, respectively. Table 2 lists the observed and calculated frequencies of some selected vibrations in sulfadiazine. To describe clearly the vibrational assignments of sulfadiazine, we summarized all vibrational fundamentals first from three groups, sulfonamide, aniline, and the pyrimidine ring. First, the sulfonamide $-SO_2NH-$ moiety is a characterized group, which can produce 114, 276, 348, 442, 566, 812, 1100, 1136, and 1318 cm^{-1} vibrational fundamentals. Among these fundamentals, the feature vibration has the strongest Raman signal at 1136 cm^{-1}, which was observed at 1148 cm^{-1} in the Raman spectrum (Figure 1c) and at 1155 cm^{-1} in the infrared spectrum in the solid state.[49] We also noticed that the fundamentals at 570, 940, and 1322 cm^{-1} can display intense infrared peaks, which can be attributed to the $-SO_2$ bending vibration, the S−N stretching vibration, and the SO_2 asymmetric stretching vibration, respectively.[50−53] The other frequencies with weak Raman signals are 281 cm^{-1} from

DOI: 10.1021/acs.jpca.9b07346
J. Phys. Chem. A 2019, 123, 9199−9208

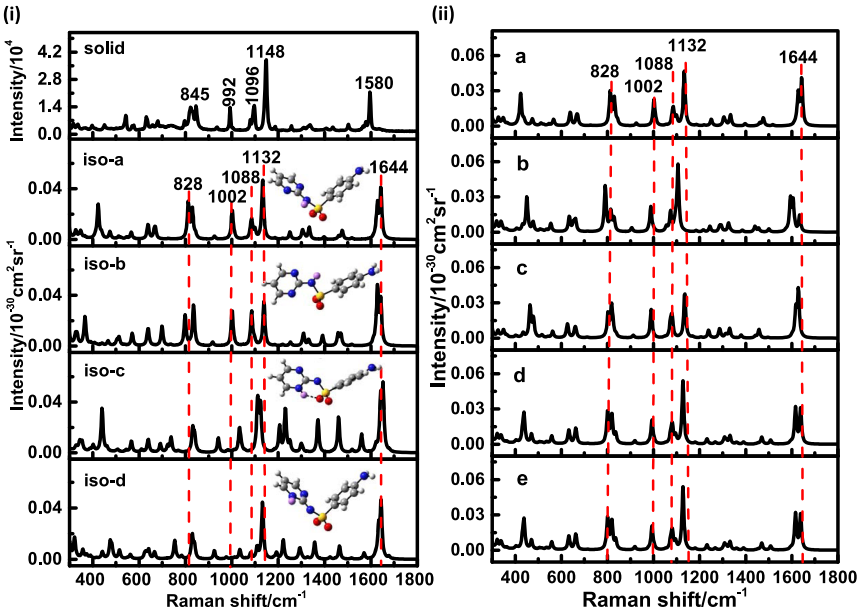

Figure 2. (i) Ordinary Raman spectra of a solid powder, and simulated Raman spectra of optimized structures as well as (ii) most stable isomer iso-a recorded by different functionals. (i) Experimental Raman spectrum of a solid powder and simulated Raman spectra of iso-a to iso-d isomers; (ii) simulated Raman spectra recorded by different functionals: (a) CAM-B3LYP, (b) B3LYP, (c) M06, (d) B3P86, and (e) MP2.

Table 1. Comparison of Selected Bond Distances Calculated Using Different Theoretical Methods with Those of Gas-Phase Electron Diffraction and Crystal Structures[a]

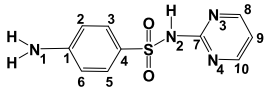

method	C−S bond length	S═O bond length	S−N bond length
GED[28]	1.770	1.432	1.682
Crystal[27]	1.736	1.440	1.643
B3LYP	1.777	1.462	1.715
CAM-B3LYP	1.764	1.445	1.692
B3P86	1.763	1.455	1.698
M06	1.764	1.452	1.692
MP2	1.7628	1.458	1.401

[a]Unit: Å.

the C−S stretching vibration, 950 cm^{-1} from the C−N stretching vibration, and 812 cm^{-1} from the torsion vibration in the pyrimidine ring.

As for the aniline moiety, the para-position-substituted group can significantly change the characteristic Raman frequencies. The υ_{8a} mode in the phenyl ring has the most intense Raman peak observed at 1595 cm^{-1} and calculated at 1644 cm^{-1}. The second strong Raman peaks include 820 and 1092 cm^{-1}, which can be attributed to the mixed vibrations between the ring-breathing motion and the C−S stretching. The other frequencies are 638 cm^{-1} from the bending vibration of the benzene ring backbone, 1215 and 1518 cm^{-1} from the symmetric C−H in-plane bending vibrations of the benzene ring, and 1306 cm^{-1} from the C−N stretching vibration. Finally, the frequency 1660−1690 cm^{-1} is attributed to the amino bending vibration, but its Raman signal is relatively weak.[54,55] In particular, we assigned the wagging vibration of the $-NH_2$ group to the Raman peak calculated at 424 (Gas) and 417 (PCM) cm^{-1}, observed at 450 cm^{-1} in the normal Raman spectrum of the solid powder. The vibrational mode strongly depends on the para-substituted group, for example, 541 cm^{-1} in aniline,[55] 461 cm^{-1} in para-fluoroaniline,[56] and 544 cm^{-1} in para-chloroaniline.[23]

For the pyrimidine ring, there are eight strong characteristic Raman peaks. The strongest Raman peak was calculated at 1628 cm^{-1} and observed at 1582 cm^{-1} in the aqueous solution (see Figure 1b), arising from the C−N symmetric stretching vibration.[57] There are three secondary intense Raman peaks calculated at 1002, 830, and 812 cm^{-1}, which can be mainly attributed to the ring deformation vibration and the ring torsion motions mixed with the C7N2 stretching. They are observed at 992, 845, and 822 cm^{-1} in the Raman spectrum of the solid powder and at 983, 826, and 818 cm^{-1} in the aqueous solution, in agreement with 986, 830, and 812 cm^{-1}, respectively. The other intense Raman peaks are predicted at 1252, 792, and 1086 cm^{-1} in the gas phase, which can be attributed to the C−N symmetric stretching vibrations, the C−H in-plane bending vibration, and the ring-breathing vibration in the pyrimidine moiety, respectively. Finally, the fundamental at 1476 cm^{-1} can be assigned to the C−N stretching vibration connected with the sulfonamide group.[58,59]

3.4. Solvation Effect and Hydrogen-Bonding Interaction. We first optimized equilibrium structures of neutral and protonated sulfadiazine with the PCM model. Figure 3 gives simulated Raman spectra of sulfadiazine and three protonated isomers with the solvation effect. Their relative Raman intensities in the low-frequency region are stronger than those in the experiment. Our vibrational analysis shows that the intense peak belongs mainly to the wagging vibration of the terminal amino group. Figure 3a shows the simulated Raman spectrum of neutral sulfadiazine. Although the solvation effect increases its Raman intensities, it has a small influence on the vibrational frequency shift. Figure 3b−d presents simulated Raman spectra of three possible protonated isomers of sulfadiazine. Among the three isomers, the simulated Raman spectrum of the terminal amino protonation isomer is the most consistent with the experimental spectrum in Figure 1b. The isomer has not only a larger relative energy

DOI: 10.1021/acs.jpca.9b07346
J. Phys. Chem. A 2019, 123, 9199−9208

Table 2. Vibrational Frequencies (Freq/cm^{-1}), Raman Activity (S_i, Å^4/amu), and Vibrational Assignment of Sulfadiazine Calculated at the CAM-B3LYP/6-311+G(d,p) Level in the Gas Phase and in the Solvation Model PCM Along with the Experimental Data

freq	scaled	PCM	S_i	IR[a]	expt[b]	assignment
1675	1642	1634	114		1595	βN_1H (27), υC_2C_3 (15), υC_5C_6 (15)
1659	1628	1624	72			υC_8N_3 (26), $\upsilon C_{10}N_4$ (23)
1504	1476	1473	17	1489	1503	υC_7N_2 (21), βN_2H (20)
1425	1398	1406	5	1404	1407	βC_8H (38), βN_2H (23), $\upsilon C_{10}N_4$ (10)
1357	1332	1343	18		1337	$\beta C_{10}H$ (19), υC_7N_2 (12)
1343	1318	1320	4			υSO (60)
1331	1306	1280	13		1284	υC_1N_1 (47), υCC in Ben (18)
1276	1252	1248	11	1258	1255	υCN in Pyrimidine(35), υN_2H (22), βC_8H (19)
1160	1136	1136	79	1152	1148	υSO (46), υC_4S (13)
1121	1100	1105	11			βC_9H (48), βC_8H (29)
1107	1086	1094	20	1089	1096	υC_8C_9 (48), $\upsilon C_{10}C_9$ (18), βC_9C_8H (13)
1100	1080	1064	8		1078	υSO (43), υC_3C_4 (15), υC_5C_4 (15)
1037	1018	1021	2			βBenzene (50), υC_1C_2 (13), υC_1C_3 (12)
1021	1002	1009	28		1004	βPyrimidine (53), υC_7N_3 (12)
1005	986	983	1	992	992	γC_3H (37), γC_5H (30), γC_2H (17), γC_6H (15)
863	850	844	4			υCC in Benzene(28) , υN_2S (10)
854	842	835	2	839		γC_1H (23), γC_6H (20), γC_1N_1 (20)
849	830	826	24		845	τPyrimidine (19), γC_7N_2 (18)
827	812	818	29		822	τPyrimidine (23), υN_2S (17), γC_7N_2 (17)
654	638	640	7	664	659	βBenzene (56), βPyrimidine (18)
651	636	637	2	635	630	βPyrimidine (50), βBenzene (23)
579	566	554	3	570	569	SO wagging (45)
450	442	436	2		468	SO rocking (27), βC_1N_1 (24), βC_4S (20)
433	424	417	11		450	N_1H_2 wagging (90)
354	348	354	2		335	SO scissoring (24), βSN_2 (13), τN_1H (13)
336	330	319	2		317	βC_7N_2 (21), υN_2S (17), γC_4S(11)
299	294	302	3			SO twisting (62)
281	276	280	6		282	υC_7S (35), βBenzene (24)
116	114		1			βN_2S (44), βC_7N_2 (15), τBen (15)

[a]Ref 49; ν, stretching; β, bending; γ, out-of-plane bending; τ, torsion; ρ, deformation. [b]The ordinary Raman spectrum of sulfadiazine in the solid powder, which is excited by a 785 nm laser.

of about 7.21 kcal/mol compared with the most stable isomer but also the remarkable change in relative Raman intensity after considering the protonation. However, the isomer can be stabilized by the intermolecular hydrogen-bonding interaction between the $-NH_2$ group and the imine in both molecules.

Next, we pay our attention to simulated Raman spectra of hydrogen-bonding dimer structures. Figure 4 presents the optimized structures of four dimers with the intermolecular hydrogen-bonding interaction (i) in the gas phase and (ii) with the PCM model. As shown in Figure 4i, these dimers have their relative energies increasing from top to bottom in the gas phase. These relative energies (see Table S3) are referred to as the 2-fold energy of the most stable isomer in Figure 2. Meanwhile, the simulated Raman spectra after considering the hydrogen bonding are more consistent with the experimental Raman spectra, and this becomes especially obvious in the low-frequency region (Figure 1). However, the intense Raman shift near 400 cm^{-1} in this region attributes to the NH_2 wagging vibration (Table 2). After further considering the PCM model, as shown in Figure 4ii, the simulated Raman spectra were further improved in the vibrational frequency and the relative Raman intensity in the middle-frequency region, in better agreement with the experimental spectra. Especially, the peaks at 828, 1006, and 1118 cm^{-1} are in better agreement with the experimental Raman peaks at 804, 1002, and 1122 cm^{-1} in Figure 1b, respectively, and it is also the most stable configuration of those dimer configurations in the PCM model. This indicates that the solvation effect influences the hydrogen-bonding interaction of the $-NH_2$ group and the Raman spectra. Additionally, we also calculated a dimer configuration with only one hydrogen bond between the terminal amino groups of two molecules (see Figure S2). There, the wagging vibrational intensity is significantly reduced.

3.5. SERS of Sulfadiazine Interacting with Gold Clusters. Different theoretical models have been used to simulate SERS spectra of probe molecules adsorbed on metal surfaces of nanoparticles, but we will use molecule-metallic cluster models here. When the metal cluster model was properly chosen and the molecule−metal interaction was better described, the Raman spectra obtained by simulations could well reproduce the SERS spectra observed in experiments. In previous SERS studies, the sulfadiazine adsorption was proposed through both oxygen atoms on silver surfaces.[48] This is based on the observation of the significant red shift of the $-SO_2$ symmetric stretching frequency. Some theoretical calculations have also been carried out to simulate the adsorption of sulfanilamide through oxygen atoms on the metal surfaces.[18] As shown in Figure 5i, we have tried to record Raman spectra of sulfadiazine interacting with a Au_4 cluster through the oxygen atoms in the $-SO_2NH-$ group. The simulated SERS spectrum is in good agreement with the reported experimental spectrum.[48] There are intense SERS peaks at 826, 1098, and 1633 cm^{-1} in Figure 5i. Their relative Raman intensities are very well reproducible with the observed SERS spectrum of sulfadiazine adsorbed on silver colloids,[48] but they are quite different from the SERS of sulfadiazine adsorbed on gold colloids (Figure 1a).

However, when sulfadiazine interacts through the amino group with a Au_4 cluster, there is a very intense Raman peak at 1012 cm^{-1} in the simulated Raman spectrum (Figure 5ii). The vibrational frequency can be assigned to the wagging vibration, but it is significantly blue-shifted compared with the observed frequency at 450 cm^{-1} for sulfadiazine in the solid powder. It is also higher than the observed SERS peak at 949 cm^{-1}, as shown in Figure 1a. In fact, the significant frequency shift of the wagging vibration was also found in aniline and para-aminothiophenol adsorbed on metal surfaces.[11,22]

To explore the nature of such an obvious difference, we also recorded spectra of sulfadiazine interacting with other gold clusters. The optimized structures and simulated Raman spectra are shown in Figure 6. When sulfadiazine interacts through the amino nitrogen with Au_2, the predicted frequency

DOI: 10.1021/acs.jpca.9b07346
J. Phys. Chem. A 2019, 123, 9199−9208

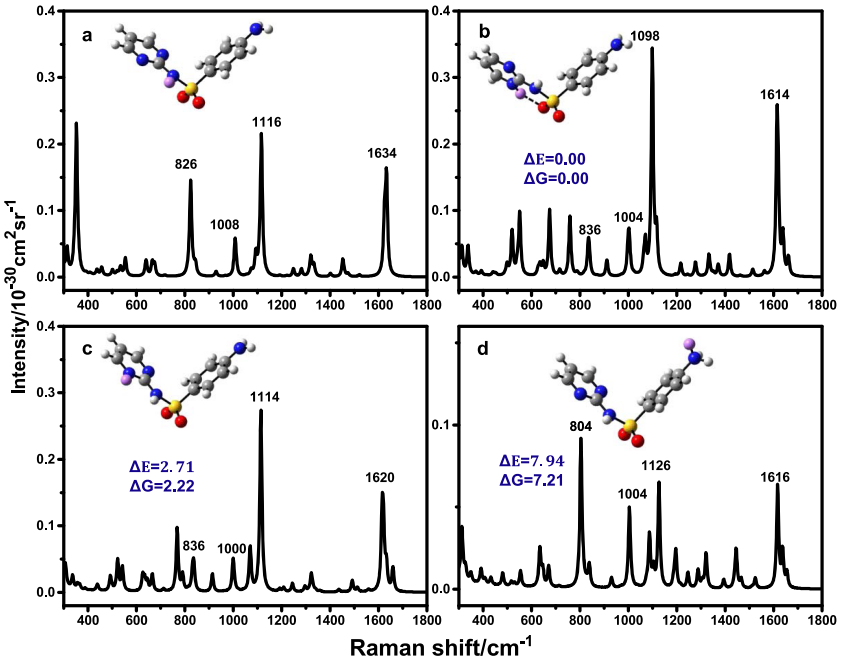

Figure 3. Simulated Raman spectra of sulfadiazine and protonated forms with the PCM model. (a) Neutral sulfadiazine; (b) protonated at the N3 atom; (c) protonated at the N4 atom; and (d) protonated at the N1 atom. ΔE and ΔG are the relative electronic energy and the relative Gibbs free energy (kcal/mol) referred to that of configuration b, respectively.

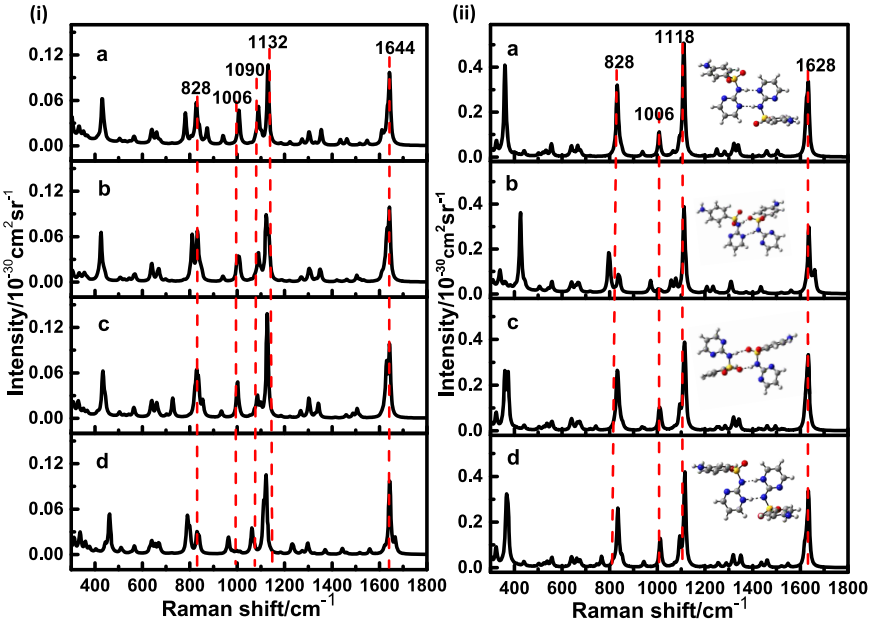

Figure 4. Simulated Raman spectra of four optimized dimer structures (i) in the gas phase and (ii) with the PCM model. (a) NHN structure with two N−H···N hydrogen bonds; (b) NHO structure with two mixed N−H···O hydrogen bonds; (c) MIX structure with N−H···O and N−H···N hydrogen bonds; and (d) isomer of NHN.

of the wagging vibration is 1002 cm^{-1}. Compared with the simulated Raman spectra mentioned above, the intense Raman peaks in Figure 6 display large red shifts to 954, 952, and 940 cm^{-1} for sulfadiazine interacting with Au_6, Au_8, and Au_{20} clusters, respectively. From the vibration analysis, the observed SERS peak at 949 cm^{-1} can be assigned to the wagging vibration originating from the $-NH_2$ out-of-plane bending motion. Table 3 summarizes the feature vibrations of the molecule adsorbed on the Au_6 cluster, and the completed vibrations are shown in Table S3. The assignment based on the PED values indicates that the wagging vibration of the amino group has a fundamental at 954 cm^{-1}, which has a very large blue shift from 424 cm^{-1} in the free molecule (see Table 2). Therefore, the binding interaction between sulfadiazine and metal clusters significantly changes the vibrational frequency and Raman intensity of the wagging vibration.

To reveal the characteristic of the wagging vibration, we further investigated it from the viewpoint of the bond strength, binding energy, molecular orbital interaction, and potential energy surfaces along the wagging vibration (see Figures S3

DOI: 10.1021/acs.jpca.9b07346
J. Phys. Chem. A 2019, 123, 9199−9208

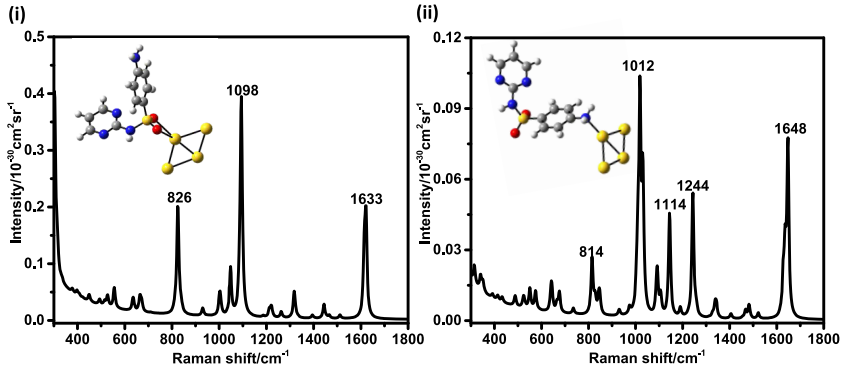

Figure 5. SERS spectra of sulfadiazine through different forms interacting with a Au_4 cluster. (i) Spectrum of sulfadiazine interacting through both O atoms; (ii) spectrum of sulfadiazine interacting through the terminal amino group.

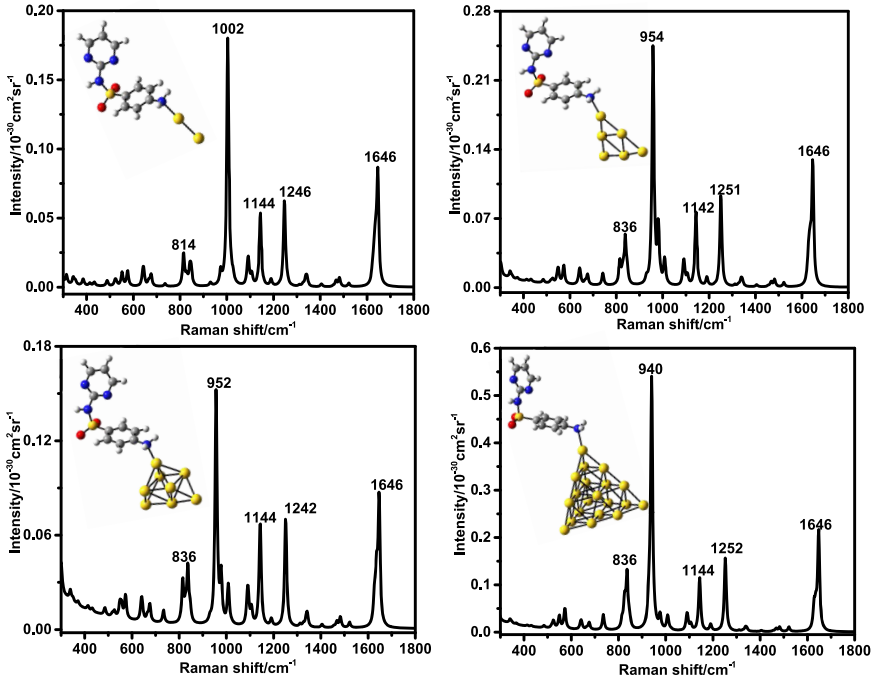

Figure 6. Simulated SERS spectra of sulfadiazine through the terminal amino group adsorbed on gold clusters.

Table 3. Selected Vibrational Frequencies of Sulfadiazine Interacting with Gold Clusters Calculated at the CAM-B3LYP/6-311+G/LANL2DZ Level**

freq	scale	expt	assignment
1679	1646	1582	νC=C in ben (60), $\beta N_{11}H$ (11)
1483	1455	1433	βSO(47), νC=C in ben (12), γC_9H(12)
1369	1343	1369	νSO(39), νC=C in ben (16), βSO(10)
1275	1251	1238	νC_1N_{11}(43) , νC=C in ben (22)
1196	1176	1181	βSO(38), γC_9H(22), $\gamma C_{10}H$(15)
1165	1142	1177	νSO(50), νC_4S(13)
1110	1089	1065	νSO(40), νC=C in ben (35)
973	954	949	NH_2 wagg (64), βSO(11)
853	836	819	$\beta C_{10}H$(37), βS=O(17), βC_7N_{12}(16), $\beta N_{12}H$(13)

and S4). Table 4 gives binding energies, N−Au bond lengths, and the wagging vibrational frequencies corresponding to different gold clusters. This indicates that the bonding strength between the metal and the molecule is strongly dependent on specific gold clusters. The bonding interaction is stronger when

Table 4. Binding Energy (E_{BE}/eV), N−Au Bond Length ($R_{N\text{-}Au}$/Å), and the Wagging Vibrational Frequency (ω/cm^{-1}) of Sulfadiazine Interacting with Different Metal Clusters

clusters	E_{BE} (eV)	R_{N-Au} (Å)	ω (cm^{-1})
Au_2	0.824	2.236	1002
Au_4	0.839	2.226	1012
Au_6	0.496	2.334	954
Au_8	0.371	2.322	952
Au_{20}	0.352	2.388	940

the amino nitrogen is binding to Au_2 and Au_4 compared with Au_6, Au_8, and Au_{20}. In the latter situations, the Raman peaks of the wagging vibration blue shift from 450 cm^{-1} in free sulfadiazine to 954 cm^{-1} (Au_6), 952 cm^{-1} (Au_8), and 940 cm^{-1} (Au_{20}). Meanwhile, the Raman intensities of the vibration become the strongest among all Raman peaks, as shown in Figure 6. It is very surprising to find these to be consistent with the experimental SERS in this study.

DOI: 10.1021/acs.jpca.9b07346
J. Phys. Chem. A 2019, 123, 9199−9208

From the viewpoint of molecular orbital interaction, the difference of the binding interaction between sulfadiazine and gold clusters can be understood well from the energy-level alignment of the molecule−metal complexes. The smaller energy gap between the interacting orbitals results in stronger bonding strength.[52] As seen in Figure 7, there are smaller

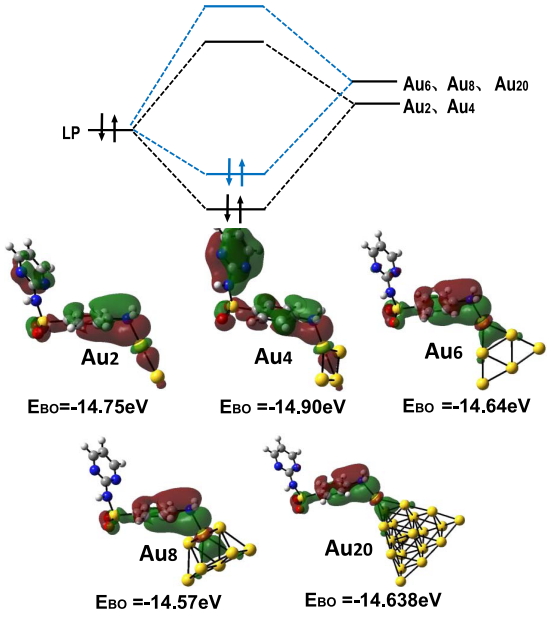

Figure 7. Orbital interaction between sulfadiazine and gold clusters as well as bonding orbitals with corresponding energy levels (E_{BO}/eV) with respect to the vacuum level.

energy gaps between the lone paired electrons in the amino nitrogen and the gold clusters (Au_2 and Au_4), and there are not only the larger binding energies but also the shorter N−Au bond distances (see Table 4). In contrast, there are smaller binding energies and larger N−Au bond distances in sulfadiazine interacting with Au_6, Au_8, and Au_{20} clusters. Thus, our calculated results provide a clearly physical picture to describe the binding interaction between the sulfadiazine amino nitrogen and metallic clusters. This also elucidates the large vibrational frequency blue shift and the very intense Raman intensity of sulfadiazine interacting with these gold clusters.

4. CONCLUSIONS

Through a combined study of experimental and theoretical investigations, we have provided deep insight into the relationship of Raman spectra and SERS on molecular structures of sulfadiazine in different environments. This should be important to understand the high detection sensitivity and interfacial Raman scattering processes in complex interfaces of nanostructures. Our experimental study provides fingerprint information at the molecular level for sulfadiazine in the solid powder, aqueous solution, and gold colloids, but it is obviously necessary to provide deep insight by combining quantum chemical calculations and normal-mode vibrational analysis. Through systematical quantum chemical calculations, we not only elucidated the stable isomer but also built the corresponding relation of its Raman spectra on stable structures. We further investigated the influence of the solvation effect, the protonation effect, and the hydrogen-bonding interaction on normal Raman spectra. We also provide a good interpretation for the unique difference in SERS spectra of sulfadiazine interacting with silver and gold surfaces. The simulated Raman spectra of sulfadiazine interacting with gold nanostructures revealed that sulfadiazine can bind to gold clusters through the terminal amino groups. This is a very interesting and unexpected phenomenon for SERS of a complex molecule such as sulfadiazine adsorbed on gold surfaces. The simulated Raman spectra are consistent with the experimental SERS, indicating that the terminal amino groups can lead to a significant frequency shift and a very intense SERS peak.

■ ASSOCIATED CONTENT

Supporting Information

The Supporting Information is available free of charge on the ACS Publications website at DOI: 10.1021/acs.jpca.9b07346.

Completed vibrational analysis of sulfadiazine and sulfadiazine adsorbed on gold clusters; configuration with only one hydrogen-bonding interaction and its Raman spectrum; calculated potential energy surface to describe the wagging vibration; and structure of sulfadiazine adsorbed on Au_4 calculated at the B3LYP/6-311+G(d,p) level (PDF)

■ AUTHOR INFORMATION

Corresponding Authors

*E-mail: guokunliu@xmu.edu.cn (G.-K.L.).
*E-mail: dywu@xmu.edu.cn (D.-Y.W.).

ORCID

Ran Pang: 0000-0001-5246-389X
Guo-Kun Liu: 0000-0003-2501-7178
De-Yin Wu: 0000-0001-5260-2861
Zhong-Qun Tian: 0000-0002-9775-8189

Notes

The authors declare no competing financial interest.

■ ACKNOWLEDGMENTS

The authors acknowledge support from the 973 Program of the Chinese Ministry of Science and Technology (Y2018YFC1602802 and 2015CB932303), the National Natural Science Foundation of China (nos 21703183, 21773197, 21533006, and 21373172), and funds of the State Key Laboratory of Physical Chemistry of Solid Surfaces and the Fujian Science and Technology Office.

■ REFERENCES

(1) Blasco, F.; Perelló, L.; Latorre, J.; Borrás, J.; Garciá-Granda, S. Cobalt(Ii), Nickel(Ii), and Copper(Ii) Complexes of Sulfanilamide Derivatives: Synthesis, Spectroscopic Studies, and Antibacterial Activity. Crystal Structure of [Co(Sulfacetamide)2(Ncs)2]. *J. Inorg. Biochem.* **1996**, *61*, 143−154.

(2) Supuran, C. T.; Mincione, F.; Scozzafava, A.; Briganti, F.; Mincione, G.; Ilies, M. A. Carbonic Anhydrase Inhibitors—Part 52. Metal Complexes of Heterocyclic Sulfonamides: A New Class of Strong Topical Intraocular Pressure-Lowering Agents in Rabbits. *Eur. J. Med. Chem.* **1998**, *33*, 247−254.

(3) Varghese, H. T.; Panicker, C. Y.; Philip, D. Vibrational Spectroscopic Studies and Ab Initio Calculations of Sulfanilamide. *Spectrochim. Acta, Part A* **2006**, *65*, 155−158.

(4) Sainz-Díaz, C. I.; Francisco-Márquez, M.; Soriano-Correa, C. Polymorphism, Intermolecular Interactions, and Spectroscopic

DOI: 10.1021/acs.jpca.9b07346
J. Phys. Chem. A 2019, 123, 9199−9208

Properties in Crystal Structures of Sulfonamides. *J. Pharm. Sci.* **2018**, *107*, 273−285.
(5) Lesch, J. E. *The First Miracle Drugs: How the Sulfa Drugs Transformed Medicine*. Oxford University Press, 2007.
(6) Ma, P.; Zhou, Z.; Yang, W.; Tang, B.; Liu, H.; Xu, W.; Huang, W. Preparation and Application of Sulfadiazine Surface Molecularly Imprinted Polymers with Temperature-Responsive Properties. *J. Appl. Polym. Sci.* **2015**, *132*, No. 41769.
(7) Haasnoot, W.; Bienenmann-Ploum, M.; Lamminmäki, U.; Swanenburg, M.; van Rhijn, H. Application of a Multi-Sulfonamide Biosensor Immunoassay for the Detection of Sulfadiazine and Sulfamethoxazole Residues in Broiler Serum and Its Use as a Predictor of the Levels in Edible Tissue. *Anal. Chim. Acta* **2005**, *552*, 87−95.
(8) Sukul, P.; Lamshöft, M.; Zühlke, S.; Spiteller, M. Sorption and Desorption of Sulfadiazine in Soil and Soil-Manure Systems. *Chemosphere* **2008**, *73*, 1344−1350.
(9) Fleischmann, M.; Hendra, P. J.; McQuillan, A. J. Raman Spectra of Pyridine Adsorbed at a Silver Electrode. *Chem. Phys. Lett.* **1974**, *26*, 163−166.
(10) John, W.; Sons, L. The Application of Surface-Enhanced Raman Spectroscopy to Identify and Quantify Chemical Adulterants or Contaminants in Foods. In *Handbook of Vibrational Spectroscopy*; Wiley, 2010.
(11) Wu, D.-Y.; Liu, X.-M.; Huang, Y.-F.; Ren, B.; Xu, X.; Tian, Z.-Q. Surface Catalytic Coupling Reaction of P-Mercaptoaniline Linking to Silver Nanostructures Responsible for Abnormal Sers Enhancement: A Dft Study. *J. Phys. Chem. C* **2009**, *113*, 18212−18222.
(12) Zhu, X.; Wang, N.; Zhang, R.; Song, W.; Sun, Y.; Duan, G.; Ding, W.; Zhang, Z.; Yang, H. Ph-Dependent Surface-Enhanced Raman Scattering Observation of Sulfanilamide on the Silver Surface. *J. Raman Spectrosc.* **2009**, *40*, 1838−1843.
(13) Lejaeghere, K.; Bihlmayer, G.; Björkman, T.; Blaha, P.; Blügel, S.; Blum, V.; Caliste, D.; Castelli, I. E.; Clark, S. J.; Dal Corso, A.; et al. Reproducibility in Density Functional Theory Calculations of Solids. *Science* **2016**, *351*, No. aad3000.
(14) Jones, R. O. Density Functional Theory: Its Origins, Rise to Prominence, and Future. *Rev. Mod. Phys.* **2015**, *87*, 897−923.
(15) Burke, K. Perspective on Density Functional Theory. *J. Chem. Phys.* **2012**, *136*, No. 150901.
(16) Zettili, N. Quantum Mechanics: Concepts and Applications. *Am. J. Phys.* **2002**, *71*, 93.
(17) Yiwei, W. X. Z.; Jun, D.; Song, H.; Jianmin, G. Studies on Interactions between Sulfadiazine and Peptide Amides. *Biotechnology* **2015**, *14*, 233−240.
(18) Castro, J. L.; Lopez-Ramirez, M. R.; Arenas, J. F.; Otero, J. C. Surface-Enhanced Raman Scattering of Benzenesulfonamide and Sulfanilamide Adsorbed on Silver Nanoparticles. *J. Raman Spectrosc.* **2012**, *43*, 857−862.
(19) Lai, K.; Zhai, F.; Zhang, Y.; Wang, X.; Rasco, B. A.; Huang, Y. Application of Surface Enhanced Raman Spectroscopy for Analyses of Restricted Sulfa Drugs. *Sens. Instrum. Food Qual. Saf.* **2011**, *5*, 91−96.
(20) Schebeliski, A. H.; Lima, D.; Marchesi, L. F. Q. P.; Calixto, C. M. F.; Pessôa, C. A. Preparation and Characterization of a Carbon Nanotube-Based Ceramic Electrode and Its Potential Application at Detecting Sulfonamide Drugs. *J. Appl. Electrochem.* **2018**, *48*, 471−485.
(21) Varghese, H. T.; Panicker, C. Y.; Anto, P. L.; Philip, D. Potential Dependent Sers Profile of Sulfanilamide on Silver Electrode. *J. Raman Spectrosc.* **2006**, *37*, 487−491.
(22) Zhao, L.-B.; Huang, R.; Bai, M.-X.; Wu, D.-Y.; Tian, Z.-Q. Effect of Aromatic Amine−Metal Interaction on Surface Vibrational Raman Spectroscopy of Adsorbed Molecules Investigated by Density Functional Theory. *J. Phys. Chem. C* **2011**, *115*, 4174−4183.
(23) Tao, S.; Yu, L.-J.; Pang, R.; Huang, Y.-F.; Wu, D.-Y.; Tian, Z.-Q. Binding Interaction and Raman Spectra of P−Π Conjugated Molecules Containing Ch2/Nh2 Groups Adsorbed on Silver Surfaces: A Dft Study of Wagging Modes. *J. Phys. Chem. C* **2013**, *117*, 18891−18903.
(24) Xu, Y.; Konrad, M. P.; Lee, W. W. Y.; Ye, Z.; Bell, S. E. J. A Method for Promoting Assembly of Metallic and Nonmetallic Nanoparticles into Interfacial Monolayer Films. *Nano Lett.* **2016**, *16*, 5255−5260.
(25) Xu, Y.; Konrad, M. P.; Trotter, J. L.; McCoy, C. P.; Bell, S. E. J. Rapid One-Pot Preparation of Large Freestanding Nanoparticle-Polymer Films. *Small* **2017**, *13*, No. 1602163.
(26) Kokila, M. K.; Puttaraja, P.; Kulkarni, M. V.; Thampi, S. 4-Amino-N-(2-Pyrimidinyl)Benzenesulfonamide. *Acta Crystallogr., Sect. C: Cryst. Struct. Commun.* **1995**, *51*, 333−336.
(27) Elacqua, E.; Bučar, D.-K.; Henry, R. F.; Zhang, G. G. Z.; MacGillivray, L. R. Supramolecular Complexes of Sulfadiazine and Pyridines: Reconfigurable Exteriors and Chameleon-Like Behavior of Tautomers at the Co-Crystal−Salt Boundary. *Cryst. Growth Des.* **2013**, *13*, 393−403.
(28) Petrov, V. M.; Girichev, G. V.; Oberhammer, H.; Petrova, V. N.; Giricheva, N. I.; Bardina, A. V.; Ivanov, S. N. Molecular Structure and Conformations of Para-Methylbenzene Sulfonamide and Ortho-Methylbenzene Sulfonamide: Gas Electron Diffraction and Quantum Chemical Calculations Study. *J. Phys. Chem. A* **2008**, *112*, 2969−2976.
(29) Becke, A. D. Density-Functional Thermochemistry. Iii. The Role of Exact Exchange. *J. Chem. Phys.* **1993**, *98*, 5648−5652.
(30) Heyd, J.; Scuseria, G. E.; Ernzerhof, M. Hybrid Functionals Based on a Screened Coulomb Potential. *J. Chem. Phys.* **2003**, *118*, 8207−8215.
(31) Lee, C.; Yang, W.; Parr, R. G. Development of the Colle-Salvetti Correlation-Energy Formula into a Functional of the Electron Density. *Phys. Rev. B* **1988**, *37*, 785−789.
(32) Tsuneda, T.; Suzumura, T.; Hirao, K. A New One-Parameter Progressive Colle−Salvetti-Type Correlation Functional. *J. Chem. Phys.* **1999**, *110*, 10664−10678.
(33) Yanai, T.; Tew, D. P.; Handy, N. C. A New Hybrid Exchange−Correlation Functional Using the Coulomb-Attenuating Method (CAM-B3LYP). *Chem. Phys. Lett.* **2004**, *393*, 51−57.
(34) Perdew, J. P. Density-Functional Approximation for the Correlation Energy of the Inhomogeneous Electron Gas. *Phys. Rev. B* **1986**, *33*, 8822−8824.
(35) Zhao, Y.; Truhlar, D. G. Density Functionals with Broad Applicability in Chemistry. *Acc. Chem. Res.* **2008**, *41*, 157−167.
(36) Altun, A.; Gölcük, K.; Kumru, M. Structure and Vibrational Spectra of P-Methylaniline: Hartree-Fock, MP2 and Density Functional Theory Studies. *J. Mol. Struct.: THEOCHEM* **2003**, *637*, 155−169.
(37) Krishnan, R.; Pople, J. A. Approximate Fourth-Order Perturbation Theory of the Electron Correlation Energy. *Int. J. Quantum Chem.* **1978**, *14*, 91−100.
(38) Pople, J. A.; Binkley, J. S.; Seeger, R. Theoretical Models Incorporating Electron Correlation. *Int. J. Quantum Chem.* **1976**, *10*, 1−19.
(39) Krishnan, R.; Binkley, J. S.; Seeger, R.; Pople, J. A. Self-Consistent Molecular Orbital Methods. Xx. A Basis Set for Correlated Wave Functions. *J. Chem. Phys.* **1980**, *72*, 650−654.
(40) McLean, A. D.; Chandler, G. S. Contracted Gaussian Basis Sets for Molecular Calculations. I. Second Row Atoms, Z = 11−18. *J. Chem. Phys.* **1980**, *72*, 5639−5648.
(41) Alkauskas, A.; Baratoff, A.; Bruder, C. Gaussian Form of Effective Core Potential and Response Function Basis Set Derived from Troullier−Martins Pseudopotential: Results for Ag and Au. *J. Phys. Chem. A* **2004**, *108*, 6863−6868.
(42) Tomasi, J.; Mennucci, B.; Cammi, R. Quantum Mechanical Continuum Solvation Models. *Chem. Rev.* **2005**, *105*, 2999−3094.
(43) Frisch, M. J.; Schlegel, H. B.; Scuseria, G. E.; Robb, M. A.; Cheeseman, J. R.; Scalmani, G.; Barone, V.; Mennucci, B.; Petersson, G. A.et al. *Gaussian 09*; Gaussian, Inc.: Wallingford, CT, 2009.
(44) Pulay, P.; Fogarasi, G.; Pang, F.; Boggs, J. E. Systematic Ab Initio Gradient Calculation of Molecular Geometries, Force Constants, and Dipole Moment Derivatives. *J. Am. Chem. Soc.* **1979**, *101*, 2550−2560.

DOI: 10.1021/acs.jpca.9b07346
J. Phys. Chem. A 2019, 123, 9199−9208

(45) Jarzecki, A. *Scale 2.0*; University of Arkansas: Fayetteville, AR, 1990.
(46) Deyin, W.; Xiumin, L.; Yifan, H.; Bin, R.; Xin, X.; Zhongqun, T. Surface Catalytic Coupling Reaction of P-Mercaptoaniline Linking to Silver Nanostructures Responsible for Abnormal Sers Enhancement: A Dft Study. *J. Phys. Chem. C* **2009**, *113*, 18212−18222.
(47) Krishnakumar, V.; Keresztury, G.; Sundius, T.; Ramasamy, R. Simulation of Ir and Raman Spectra Based on Scaled Dft Force Fields: A Case Study of 2-(Methylthio)Benzonitrile, with Emphasis on Band Assignment. *J. Mol. Struct.* **2004**, *702*, 9−21.
(48) Sutherland, W. S.; Laserna, J. J.; Angebranndt, M. J.; Winefordner, J. D. Surface-Enhanced Raman Analysis of Sulfa Drugs on Colloidal Silver Dispersion. *Anal. Chem.* **1990**, *62*, 689−693.
(49) Sinisterra, R. D.; Najjar, R.; de Oliveira, L. F. C. A Raman Spectroscopic Investigation of Sulphadiazine and of Its Dirhodium Tetracarboxylate Adducts. *Spectrosc. Lett.* **1993**, *26*, 305−318.
(50) Philip, D.; Eapen, A.; Aruldhas, G. Vibrational and Surface Enhanced Raman Scattering Spectra of Sulfamic Acid. *J. Solid State Chem.* **1995**, *116*, 217−223.
(51) Ogruc Ildiz, G.; Akyuz, S. Conformational Analysis and Vibrational Study of Sulfanilamide. *Vib. Spectrosc.* **2012**, *58*, 12−18.
(52) Borba, A.; Gómez-Zavaglia, A.; Fausto, R. Conformational Landscape, Photochemistry, and Infrared Spectra of Sulfanilamide. *J. Phys. Chem. A* **2013**, *117*, 704−717.
(53) Vinod, K. S.; Periandy, S.; Govindarajan, M. Spectroscopic [Ft-Ir and Ft-Raman] and Molecular Modeling (Mm) Study of Benzene Sulfonamide Molecule Using Quantum Chemical Calculations. *J. Mol. Struct.* **2016**, *1116*, 226−235.
(54) Wang, H.; Wu, G. The Electronic Structures of the Nonresonant Raman Excited Virtual States of 2-Aminopyridine by 632.8 and 514.5 nm Excitations as Evidenced by the Bond Polarizabilities. *Chem. Phys. Lett.* **2006**, *421*, 460−463.
(55) Wojciechowski, P. M.; Zierkiewicz, W.; Michalska, D.; Hobza, P. Electronic Structures, Vibrational Spectra, and Revised Assignment of Aniline and Its Radical Cation: Theoretical Study. *J. Chem. Phys.* **2003**, *118*, 10900−10911.
(56) Wojciechowski, P. Theoretical Anharmonic Raman and Infrared Spectra with Vibrational Assignments and Nbo Analysis for 2,3,4,5,6-Pentafluoroaniline. *J. Fluorine Chem.* **2013**, *154*, 7−15.
(57) Prabavathi, N.; Nilufer, A.; Krishnakumar, V.; Akilandeswari, L. Spectroscopic, Electronic Structure and Natural Bond Analysis of 2-Aminopyrimidine and 4-Aminopyrazolo[3,4-D]Pyrimidine: A Comparative Study. *Spectrochim. Acta, Part A* **2012**, *96*, 226−241.
(58) Akyüz, S.; Akyüz, T.; Davies, J. E. D. Ft−Ir and Ft−Raman Spectroscopic Investigations of Adsorption of 2-Aminopyridine on Natural and Ion-Exchanged Bentonites. *J. Mol. Struct.* **1999**, *482*−*483*, 49−52.
(59) Jose, S. P.; Mohan, S. Vibrational Spectra and Normal Co-Ordinate Analysis of 2-Aminopyridine and 2-Amino Picoline. *Spectrochim. Acta, Part A* **2006**, *64*, 240−245.

DOI: 10.1021/acs.jpca.9b07346
J. Phys. Chem. A 2019, 123, 9199−9208